Applied Catalysis B: Environmental 170-171 (2015) 263–272

Contents lists available at ScienceDirect

Applied Catalysis B: Environmental

journal homepage: www.elsevier.com/locate/apcatb

# Impact of the spatial distribution of sulfate species on the activities of $SO_4^{2-}/TiO_2$ photocatalysts for the degradation of organic pollutants in reverse osmosis concentrate

Xuan Hao Lin [a], Sam Fong Yau Li [a,b,*]

[a] Department of Chemistry, National University of Singapore, 3 Science Drive 3, 117543, Singapore
[b] NUS Environmental Research Institute (NERI), #02-01, T-Lab Building (TL), 5A Engineering Drive 1, Singapore 117411, Singapore

ARTICLE INFO

*Article history:*
Received 15 December 2014
Received in revised form 28 January 2015
Accepted 2 February 2015
Available online 3 February 2015

*Keywords:*
Sulfated titanium dioxide
Photocatalytic activity
Reverse osmosis concentrate
Band gap
Electron trapping

ABSTRACT

Sulfate ions bonded to titanium ions on the surface of internally sulfated $TiO_2$ greatly improved its photocatalytic activity for the degradation of organic pollutants in reverse osmosis concentrate (ROC). The catalysts were characterized with XRD, BET, SEM, FTIR, EDS, UV–vis DRS, ICP/MS, XPS and Mott-Schottky plots etc. For the activity difference of sulfated $TiO_2$ (S-TO) catalysts, reasons on crystal phase, primary particle size, surface area (SA), pores, band gap ($E_g$), microscopy morphology and Brönster acid sites were ruled out. The activity difference of S-TO catalysts was attributed to the spatial distribution of sulfate species. Sulfate species on the S-TO catalysts functioned as electron traps. Surface sulfate species improved activity while bulk core sulfate species hindered it. Based on XPS Ti 2p binding energy (BE) and measured $E_g$ from UV–vis DRS, band positions of catalysts were calculated illustrating electron trapping and transferring. Sulfate ions lowered the energies of both CB and VB of S-TO catalysts compared with the pure anatase $TiO_2$.



## 1. Introduction

Reverse osmosis (RO) membrane technology has been widely applied in wastewater recovery processes and desalination processes. Currently only 75–85% of feed water can be purified as clean product water by utilizing RO membrane for wastewater recovery. The remaining 15–25% of reverse osmosis concentrate (ROC) is brackish waste [1]. ROC has light yellow appearance and high organic and inorganic content which would increase the chance of membrane fouling and power consumption due to higher working pressure. Without efficient and cost-effective purification technologies, ROC is commonly discharged to water bodies, which poses a potentially serious threat to marine ecosystems due to high organic content [2]. Many efforts have been made to reclaim clean water from the ROC, while results are still not satisfactory [3–5]. Besides conventional treatment methods such as activated carbon adsorption, coagulation, air stripping, chemical oxidation (e.g. chlorination or ozonation), and relatively new microbial fuel cells [6], recently advanced oxidation processes (AOPs) through combination of a few methods such as photocatalysis and chemical oxidation have drawn much attention. However, the AOP methods for ROC treatment are still not satisfactory due to low degradation ratio, harmful by-products or slow degradation speed [7,8]. For ROC reclamation, key requirements include high efficiency, low cost, environmental friendly final products, long catalyst life, and cost-effective regeneration methods. Here we report sulfated $TiO_2$ catalysts with these key features.

$TiO_2/SO_4^{2-}$ solid superacid has been used as catalysts for a variety of organic reactions [9–12]. It showed an increased photoactivity for several substrates, such as ethylene, hexane, methanol, benzene, and trichloroethylene (TCE). Sulfation of the catalyst led to an increase of the surface acidity and an increase of adsorption strength and therefore improvement of the adsorption coverage of the substrates. Sulfation is usually achieved by impregnation of $TiO_2$ using 1 M $H_2SO_4$. The Brønsted acid sites are believed to be responsible for the high levels of acidity and catalytic activity in sulfated $ZrO_2$ or $TiO_2$ [13]. Also, in sulfated titania, the O=S=O groups anchored to the surface are coordinated with water, thus inducing electron deficient sulfur species which may act as electron traps [14]. An improvement of the anatase thermal stability, against sintering was shown; the anatase phase was preserved up to 700 °C with relatively high surface area with respect to the non-

* Corresponding author. Tel.: +65 6515 2681; fax: +65 6779 1691.
*E-mail address:* chmlifys@nus.edu.sg (S.F.Y. Li).

http://dx.doi.org/10.1016/j.apcatb.2015.02.001
0926-3373/

sulfated $TiO_2$ [13,15]. However, at such temperatures, the $SO_4^{2-}$ content should be negligible, as it is well known that sulfate groups would be stable only up to 600 °C during calcination. This high calcination temperature (700 °C) tended to eliminate crystal defects, which could be responsible for preventing the electron-hole recombination process, and therefore lowered the efficiency. Increase in the photocatalyst life was also evidenced for sulfated samples [16]. Nevertheless, all reported sulfation of $TiO_2$ were conducted as a post-treatment with externally added reagents after $TiO_2$ had been formed. Here we reported an internally sulfated $TiO_2$ photocatalysts with high efficiency. No external sulfate ions were added. Internal sulfation was accomplished when $TiO_2$ catalysts were formed and the sulfate ions originated from the $TiO_2$ precursor. Internal sulfation is a simultaneous sulfation and formation process. In this work we investigated sulfate species on the internally sulfated $TiO_2$ and reported the impact of spatial sulfate distribution on the photocatalytic activity.

## 2. Experimental

### *Materials*

Titanyl sulfate (99.5%, AR), ethanol (95%, Reagent grade), absolute ethanol (99.9%, AR grade), ammonia 25% (AR grade) were obtained from Sigma–Aldrich. ROC was obtained from a Singapore water treatment plant. Characteristics of ROC were listed in Supplementary information (SI) Table S1.

### *Preparation of catalysts*

S-TO photocatalysts (E33W67–hydrolysed in 33%v/v ethanol and 67% water; and E80W20–hydrolysed in 80% ethanol and 20% water) were prepared through $TiO_2$ precursor hydrolysis in ethanol/water solution with various ethanol/water ratios as we reported [17,18].

### *Degradation of organic pollutants in ROC*

Photocatalytic reactions of ROC were conducted under monochromatic UV 365 nm irradiation (18 mW/cm$^2$; 6.467 $\times 10^{15}$ photons/s·ml) over 0.1%wt S-TO catalysts in a quartz reactor with temperature control at 25+/− 0.2 °C (SI Fig. S1). ROC samples before and after reaction were analysed by liquid chromatography–quadrupole time of flight (LC–QToF) tandem mass spectrometry, fluorescence spectroscopy, TOC analyzer and GC/MS (SI Fig. S2, S3, S4). However, no volatile organic compounds were detected (SI Fig. S5).

### *Characterization of catalysts*

The S content in the catalysts were measured by energy dispersion spectroscopy EDS and X-ray photoelectron spectroscopy (XPS). Surface area and isotherm were measured by $N_2$ sorption. Crystal phases and sizes were measured by XRD. Morphology was visualized by SEM and TEM (SI Fig. S6). Band gaps were measured by UV–vis diffuse reflectance spectroscopy (DRS) (SI Fig. S7, Table S2). Chemical bonding between sulfate and Ti(IV) was confirmed by FTIR. Surface compositions and Ti, O, S species were measured by XPS (SI Fig. S8, S9, S10, Table S3). For catalyst band gap measurement, UV–vis DRS spectra of powder samples were recorded on Shimadzu 2450 diffuse reflectance UV–visible spectrophotometer. FTIR spectrum was carried out using Shimadzu IR Prestige 21. FTIR samples were pre-treated at 80 °C for 8 h to get rid of adsorbed moisture. KBr was baked at 130 °C for 24 h. KBr pellet was done on Shimadzu KBr pellet press equipped with a vacuum pump. The powder sample was vacuumed for 5 min and then pressed at 78.5 kN pressure with continuous vacuum for 15 min. Sample concentration in KBr powder was 0.5–1%wt. Background spectrum was recorded on pure KBr pellet in air at room temperature 25 °C and was subtracted from the sample spectrum at the same temperature. The IR spectra were recorded by accumulating 32 scans at a spectral resolution of 4 cm$^{-1}$. XPS was carried out using Omicron analyser EA125 7-channel spectrometer. The radiation source was monochromatic Mg Kα radiation operating at a power of 300 W (15 kV, 20 mA). Analysis chamber vacuum pressure was $4.3 \times 10^{-9}$ Torr. Samples were pre-vacuumed for overnight to ensure adsorbed species were removed. During measurement, constant analyser energy modes (CAE) for wide scan and elemental scan were 50 eV (bigger slit) and 20 eV (smaller slit), respectively. Emission angle was 15°. Equipment work function $\Phi_{spec}$ = 4.42 eV. Curve fitting was done on software XPSPEAK41 (SI). Other techniques including ICP/MS and Mott–Schottky plots (SI Fig. S11) are listed in SI.

## 3. Results

### 3.1. Characterization

#### 3.1.1. XRD

All S-TO photocatalysts were pure anatase, their XRD patterns are shown in Fig. 1a. The lattice planes included (101), (004), (200), (105), (211) and (118). S-TO catalysts prepared from ethanol/water mixture with higher water content had higher crystallinity (Fig. 1a). The broaden peaks indicated the crystal particles were in nano-sizes. For nano-size powder, XRD peaks broaden due to insufficient diffraction planes to cancel the intensity outside the peak centers (Bragg's angle). The size of the nano-particles (Table 1)

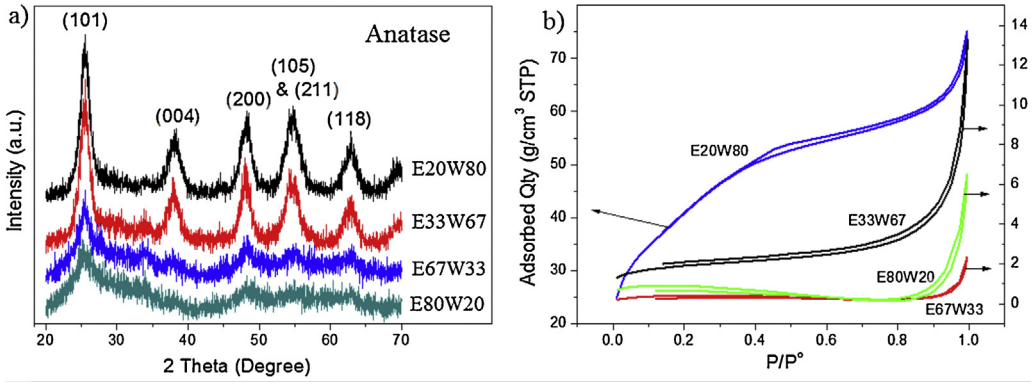


**Fig. 1.** (a) XRD patterns and (b) $N_2$ adsorption/desorption isotherms of the S-TO photocatalysts E20W80, E33W67, E67W33 and E80W20.

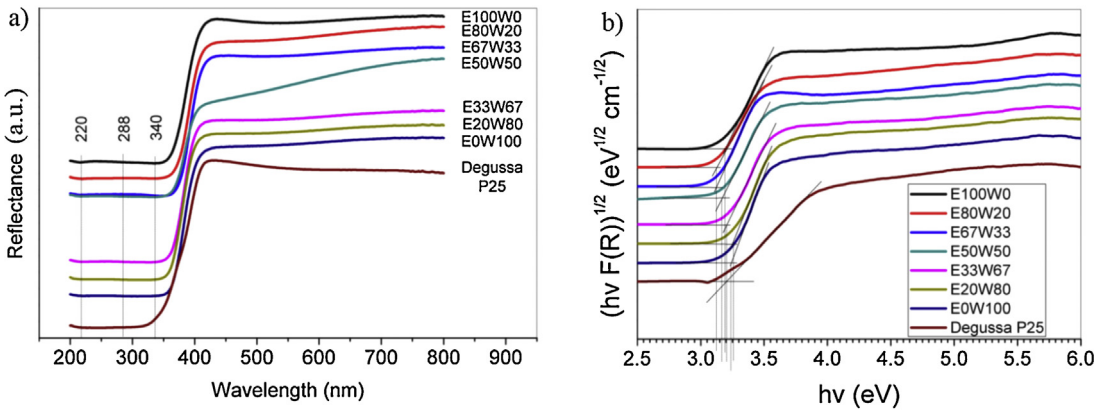


**Fig. 2.** (a) UV–vis DRS and (b) Tauc plots for the indirect allowed bandgaps of S-TO photocatalysts E0W100, E20W80, E33W67, E50W50, E67W33, E80W20, E100W0 and Degussa P25 $TiO_2$.

could be calculated from the XRD data using the Scheller's formula [9–12]. The size range was 4–7 nm.

### 3.1.2. BET

The $N_2$ adsorption/desorption isotherms of the S-TO photocatalysts are shown in Fig. 1b. E33W67, E67W33 and E80W20 showed reversible type III isotherms, while E20W80 showed reversible type II isotherms. Reversible type III isotherms are not common where the adsorbent–adsorbate interactions play an important role. Type II isotherm is the normal form of isotherm obtained with non-porous or macroporous adsorbents. The Type II isotherm represents unrestricted monolayer-multilayer adsorption and has Point B (the beginning of the almost linear middle section of the isotherm, is often taken to indicate the stage at which monolayer coverage is complete and multilayer-adsorption about to begin). BET surface areas were calculated and listed in the Table 1. E33W67, E67W33 and E80W20 had low surface areas (<10 $m^2/g$) while E20W80 had high surface areas (>140 $m^2/g$). Higher surface areas usually had advantages for DOC adsorption and its further degradation, but did not ensure the photocatalytic activity. Adsorption was only one of the steps in the photocatalytic reaction, however, may not be the control step.

### 3.1.3. UV–vis DRS

Fig. 2a shows the UV–vis DRS spectra of all S-TO photocatalysts and Degussa P25 $TiO_2$. At 220 and 288 nm there were charge transfers from $O^{2-}$ to $Ti^{4+}$. 340 nm was an interband transition for anatase. The S-TO photocatalysts absorbed less lights at 350–450 nm. Indirect allowed bandgaps (Table 1) were derived from Tauc plots calculated using Tauc functions (SI Fig. S7 and Table S2). Bandgaps of all S-TO catalysts were in the range of 3.10–3.30 eV, indicating they were typical UV photocatalysts. There were no significant differences among the bandgaps of all S-TO photocatalysts.

### 3.1.4. SEM, EDS

All S-TO photocatalysts appeared to be white powder to the naked eyes. The SEM photographs of E33W67 and E80W20 (Fig. 3a and c) indicated that the primary particles (4–7 nm) formed aggregates or agglomerates, i.e. secondary particles in a size range of 0.1–3 μm. There were no significant difference of the appearance of E33W67 and E80W20 under SEM. EDS spectra of S-TO catalysts (Fig. 3b and d) showed that they contained some S content.

### 3.1.5. ICP/MS

S content of the catalysts were quantified by ICP/MS (Fig S10, Table 2). E0W100, E20W80 and E33W67 prepared from the ethanol/water mixture with less ethanol content had relatively low S content, while the other S-TO photocatalysts prepared from the ethanol/water mixture with less water content had relatively high S content (Table 2). Main forms of S content were sulfate species. S content in bulk core mainly existed as sulfate ions, which may exist as chelating bidentate $SO_4^{2-}$ ions, bridged bidentate $SO_4^{2-}$ ions, and interstitial $SO_4^{2-}$ ions (Fig. 4).

### 3.1.6. TEM

TEM image of the S-TO sample E20W80 proved that they were composed of primary sphere shape nano-size particles (Fig. S6a). High resolution TEM image (HRTEM) of E20W80 (Fig. S6b) showed an atomic array of crystal planes (200) along the direction [002]. The measured $d_{(200)}$ spacing (0.189 nm) from both HRTEM and selected area electron diffraction (SAED; Fig. S6c) was consistent with the results from XRD.

## 3.2. Photocatalytic performance

According to our preliminary studies, the original ROC sample contained humic substances 23.36 ppm (95.35%wt), 63 surfactants 1.08 ppm (4.41%wt) and 9 drug residues 0.06 ppm (0.24%wt), with a total DOC 24.50 ppm [17,18]. S-TO catalyst E33W67 with S content 4.79%wt had higher efficiency in degrading organic pollutants in ROC than Degussa P25 (Fig. 5a). While E80W20 with higher S content 8.94%wt was not as efficient as Degussa P25. Since E33W67 was sulphated $TiO_2$, it is common to assume that its high activity might originate from Brönsted acid sites. However, after its Brönsted acid sites (2.58 mmol/g) were completed neutralized, its activity was even better ($C/C_0$ 14.91%) than before ($C/C_0$ 27.11%) (Fig. 5b). To explain the activity difference of E33W67 and E80W20, we investigated the possible reasons of crystal phase, primary particle size,

**Table 1**
Physical properties and activities of S-TO photocatalysts.

| Sample | Ethanol/Water ratio (v/v) | Surface area ($m^2/g$) | Crystal size (nm) | Band gap $E_g$ (eV) | Conversion of DOC in ROC at 6 h (%) |
|---|---|---|---|---|---|
| E80W20 | 80/20 | 2.86 | 4.82 | 3.260 | 3.8 |
| E67W33 | 67/33 | 1.40 | 5.04 | 3.205 | 10.8 |
| E33W67 | 33/67 | 6.67 | 6.30 | 3.125 | 72.9 |
| E20W80 | 20/80 | 146.90 | 6.40 | 3.125 | 76.8 |

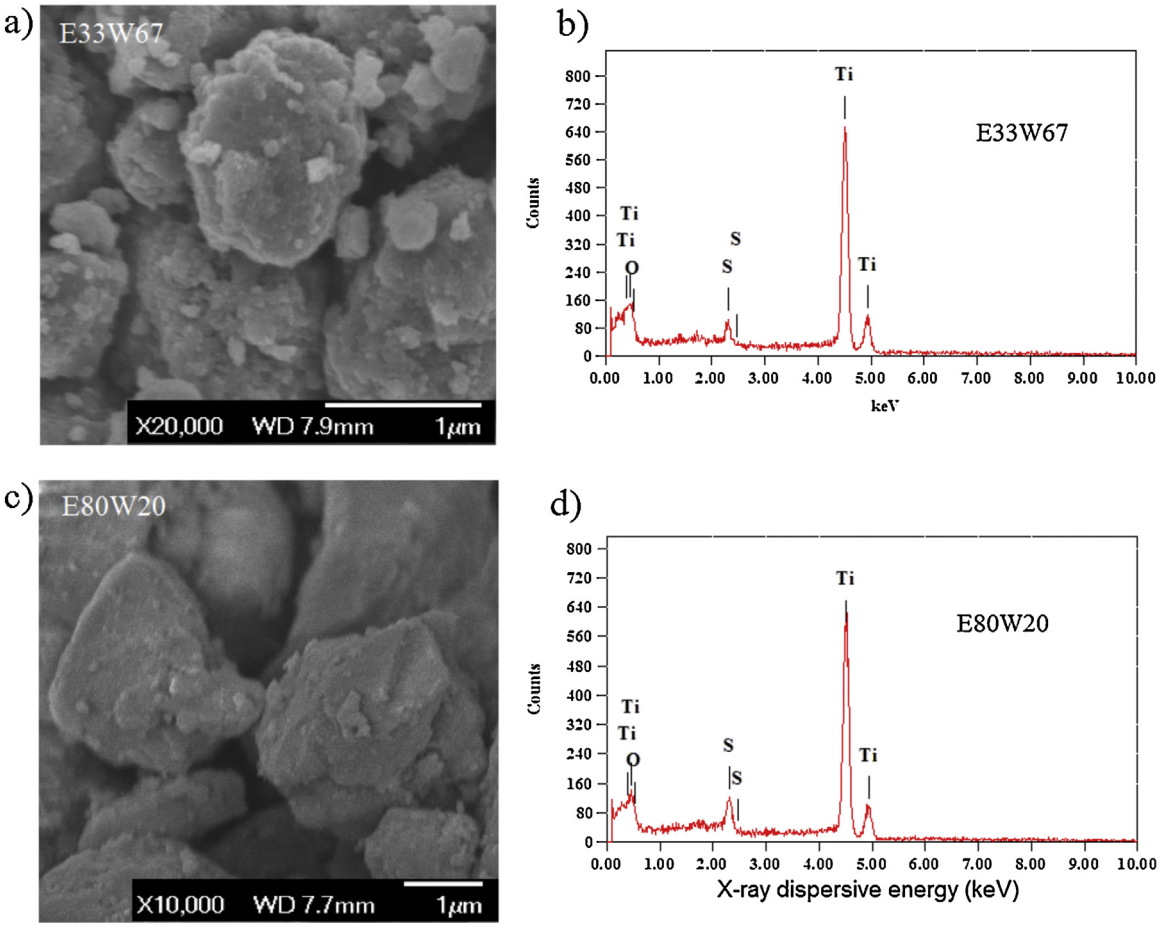


**Fig. 3.** (a) SEM photograph and (b) EDS spectrum of S-TO photocatalyst E33W67; (c) SEM photograph and (d) EDS spectrum of S-TO photocatalyst E80W20

SA, pores, microscopy morphology, $E_g$ and Brönsted acid sites (Fig. S13). Since they had same crystal phase, and similar primary particle size, SA, pores, microscopy morphology and $E_g$, in addition, Brönsted acid sites did not enhance the activity of E33W67, we ruled these possible factors.

### 3.3. XPS

Surface S:Ti atomic ratios for E80W20 and E33W67 were 48.9:100 and 47.1:100, respectively (Table 3). S:Ti ratios calculated from XPS were much higher than that (13.4:100, 27.9:100) measured from ICP/MS. XPS results represented surface 3–10 nm in depth but ICP/MS results represented the total S concentration. It implied that surface S:Ti ratio was different from that in bulk core (underneath the surface). From the surface area, surface S:Ti ratio, and the total S content measured by ICP/MS, the S:Ti ratios in the bulk core were calculated to be 12.13:100 and 27.57:100 for E33W67 and E80W20, respectively (SI). E33W67 had a low bulk core S:Ti ratio 12.13:100 and high surface S:Ti ratio 47.1:100. While E80W20 had a relatively high bulk core S:Ti ratio 27.57:100 (more than double of that of E33W67) and high surface S:Ti ratio 48.9:100. Surface to bulk core S content ratio could also be calculated to be 3.88/1 and 1.77/1 for E33W67 and E80W20, which indicated that E33W67 had a higher surface to bulk core sulfate content ratio than E80W20. Low bulk core S:Ti ratio 12.13:100 in E33W67 and relative high bulk core S:Ti ratio 27.57:100 explained the higher crystallinity (stronger peak intensity) of E33W67 and low crystallinity (weak peak intensity) of E80W20, which could be originated from the low and high aqueous $[SO_4^{2-}]$ in ethanol/water mixture during synthesis.

Ti 2p spectra were fitted into a total 7 Ti (IV) species (Fig. 6a), species assignment were listed in Fig. 6b. Ti (III), usually located at $456.0 \pm 1.0$ eV, was not detected in either sample [19]. O 1s spectra were fitted into 11 oxygen species (Fig. 6c), species assignment were listed in Fig. 6d. S 2p spectra were fitted into 5 S species (Fig. 6e), their assignment were listed in Fig. 6f. Photocatalytic reaction mechanism on $TiO_2$ has been widely accepted as electron-hole pairs separation, electron and hole capture/trap, hydroxyl (OH) radicals generation, and organics mineralization by OH radicals [20]. However, it is also common that electron-hole pairs recombine back to photons through irradiative recombination inside the lattices of $TiO_2$ with the lack of electron or hole traps, or recombine through non-irradiative recombination. Non-radiative recombination includes both single-carrier trapping due to rapid carrier relaxation into the deep states and Auger recombination. Auger recombination is a three

**Table 2**
S contents of all S-TO photocatalysts determined by ICP/MS. All RSD were within 3.0%.

| Samples | E0W100 | E20W80 | E33W67 | E50W50 | E67W33 | E80W20 | E100W0 |
|---|---|---|---|---|---|---|---|
| Preparation conditions – ratio of ethanol/water | 0/100 | 20/80 | 33/67 | 50/50 | 67/33 | 80/20 | 100/0 |
| S Content (%wt) | 3.34 | 3.79 | 4.79 | 6.34 | 8.25 | 8.94 | 15.76 |

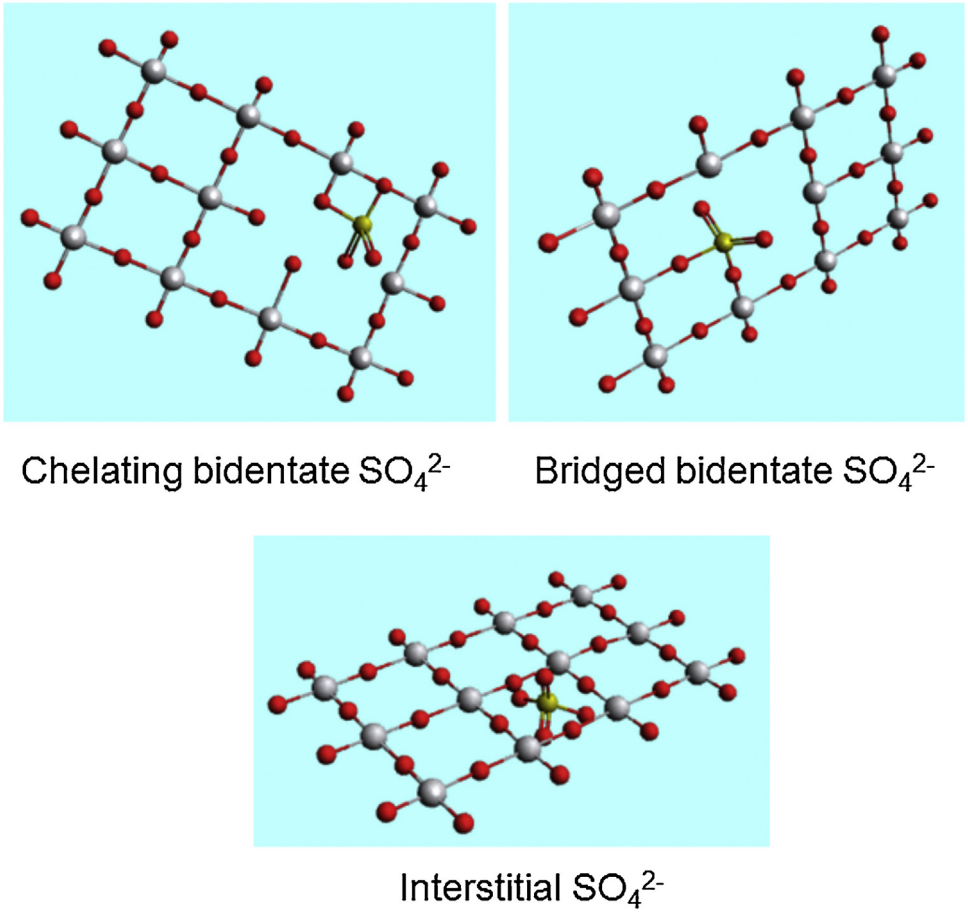


**Fig. 4.** Illustration of types of $SO_4^{2-}$ ions inside the lattices of bulk S-TO photocatalysts, (a) chelating bidentate $SO_4^{2-}$ ions; (b) bridged bidentate $SO_4^{2-}$ ions; (c) interstitial $SO_4^{2-}$ ions

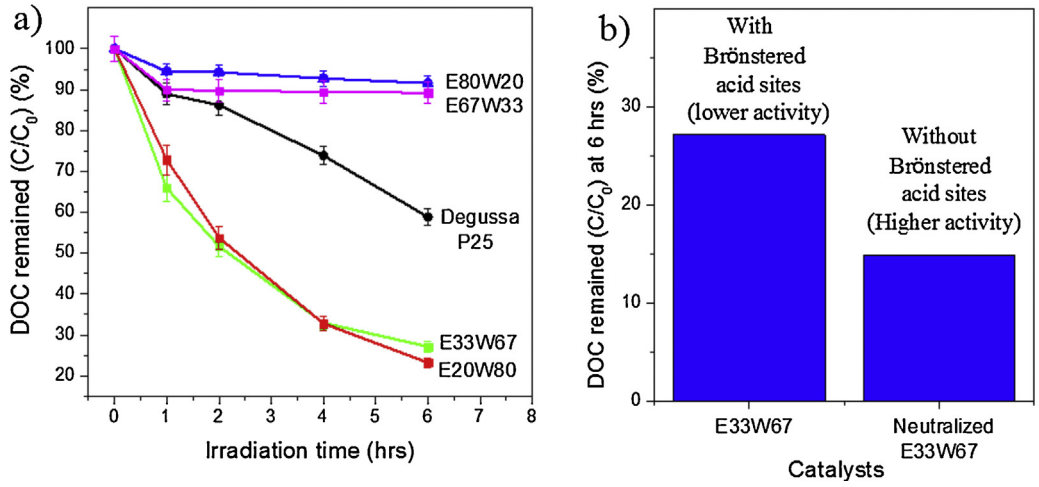


**Fig. 5.** (a) Dissolved organic content (DOC) remained in ROC with S-TO catalysts and commercial Degussa P25 after 1–6 h UV irradiation; (b) E33W67 had more Brönsted acid sites than neutralized E33W67, but neutralized E33W67 had better activity than E33W67

**Table 3**
Surface and bulk core S/Ti ratio of $SO_4^{2-}/TiO_2$ photocatalysts E33W67 and E80W20 and their surface/bulk core S ratio.

| $SO_4^{2-}/TiO_2$ | S/Ti atomic ratio | | S content* | SA** | S/Ti atomic ratio | | Surface/bulk core S ratio |
|---|---|---|---|---|---|---|---|
| | XPS | ICP/MS | (%wt) | ($m^2$/g) | Surface | Bulk core | |
| E33W67 | 47.1/100 | 13.4/100 | 4.79 | 6.67 | 47.1/100 | 12.13/100 | 3.88/1 |
| E80W20 | 48.9/100 | 27.9/100 | 8.94 | 2.86 | 48.9/100 | 27.57/100 | 1.77/1 |

* S content determined by ICP/MS.
** SA – surface area determined by $N_2$ sorption.

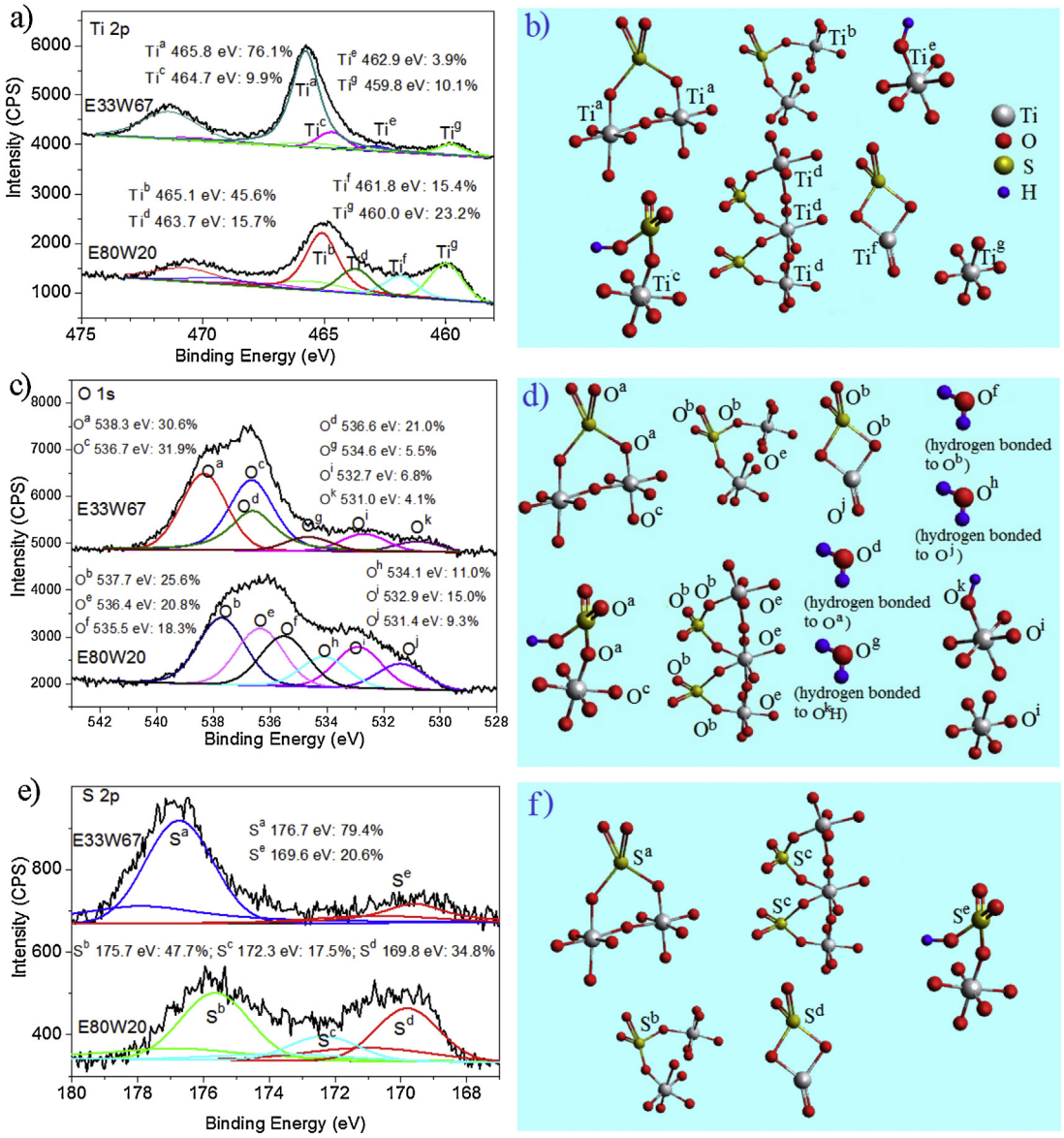


**Fig. 6.** XPS curve fittings and surface species of S-TO photocatalysts E33W67 and E80W20; (a) Ti2p, e.g. Ti $2p_{3/2}$ and $2p_{1/2}$, (b) illustration of 7 Ti species, (c) O 1s, (d) illustration of 11 O species, (e) S 2p, e.g. S $2p_{3/2}$ and $2p_{1/2}$, (f) illustration of 5 S species

particles (electron-hole-electron, electronhole-hole) process; the non-radiative recombination energy of electron-hole pairs is transferred to the kinetic energy of another electron or hole [21,22].

### 3.4. Spatial distribution of sulfate species

According to our calculation (SI), E33W67 had 12.7% population of sulfate species distributed on the surface of secondary micron size particles (average $d = 1.15\,\mu m$), and 87.3% sulfate species in the bulk core (Fig. 7). However, E80W20 had as low as only 2.72% population of sulfate species distributed on the surface of secondary micron size particles (average $d = 2.69\,\mu m$), and 97.28% sulfate species in the bulk core. E33W67 and E80W20 had similar density of sulfate species 2.77 and 2.87 species/$nm^3$ at the surface, while E80W20 had almost twice denser of sulfate species (1.623 species/$nm^3$) in the bulk core than E33W67 (0.714 species/$nm^3$). Sulfate species on the S-TO catalysts worked as electron traps. Mobility of the free photo-excited electrons were fast enough ~1 nm/ps [23], while the electron trapping time was ~500 ps with the dense sulfate species densities from 0.714 to 2.87 species/$nm^3$, the electron trapping time was the majority and the electron free transit time could be neglected. Photo-excited electrons could move from one trap to another trap by hopping [23]. Since the electron trapping time was the majority, the distribution of photo-excited electrons was mainly regulated by the spatial distribution of sulfate species. For E33W67, since it has 12.7% population of sulfate species at the surface, around 12.7% of photo-excited electrons will be trapped and utilized at the surface. While for E80W20 only 2.72% of photo-excited electrons will be trapped and utilized at the surface. This indicated E33W67 had 4.7 times more of photo-excited electrons than E80W20 at the surface available for the generation of OH radicals. Due to high percentage 97.28% of photo-excited electrons were trapped in the bulk core, electron charges easily accumulated up in E80W20, causing the whole particle potential and VB potential to lower positions, obstructing the ability to oxidize the organic pollutants in ROC.

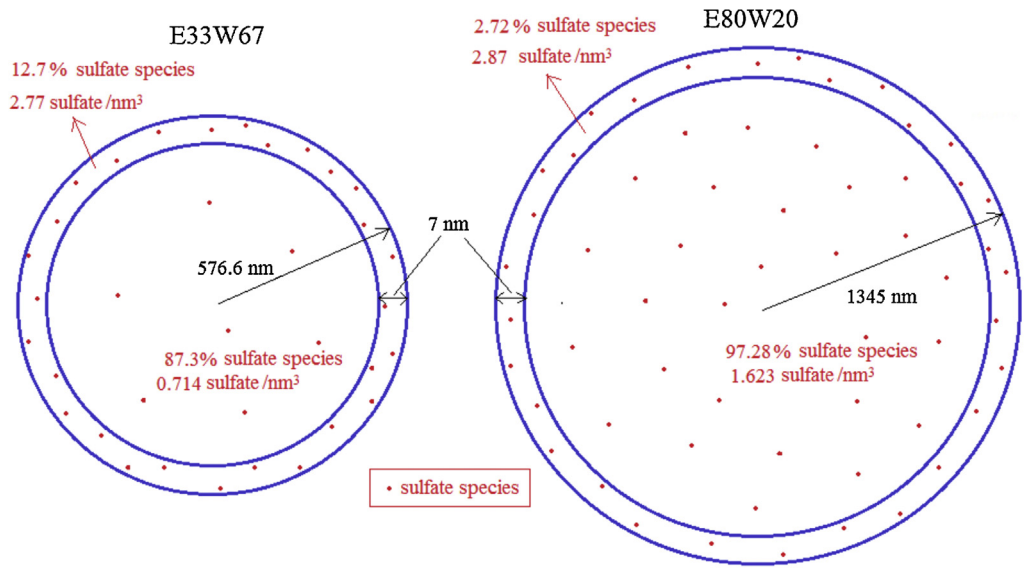


**Fig. 7.** Spatial distribution of sulfate species on the surface and bulk core of E33W67 and E80W20

### 3.5. Correlation of activity and spatial sulfate distribution

Through experimental condition control, we achieved different percentages of surface and bulk core sulfate species population. The DOC degradation efficiency by S-TO catalysts @ 6 h UV irradiation strongly correlated and was proportional with the percentage of surface sulfate species (Fig. 8a); the correlation equation was derived and shown in Eq. (1). The DOC degradation efficiency by S-TO catalysts also strongly correlated but was reversely proportional with the ratio of bulk core and surface sulfate species (Fig. 8b); the correlation equation was derived and shown in Eq. (2). In Eqs. (1) and (2), $C_0$ was the initial DOC concentration (ppm) in ROC, $C$ was the DOC concentration (ppm) in ROC after a certain time period (6 h) of UV irradiation with S-TO catalysts, $N_{surf}$ was the population of sulfate species at the surface of a secondary catalyst particle (aggregate/agglomerate) (see SI), $N_{bc}$ was the population of sulfate species in the bulk core of a secondary catalyst particle. A and B were constants, in our S-TO catalysts, 22.90 and −2.13, respectively. Eq. (2) was better than Eq. (1) due to higher $R^2$ value and simpler equation.

$$\frac{C_0 - C}{C_0} = A \ln\left(\frac{N_{surf}}{N_{surf} + N_{bc}}\right) \quad (1)$$

$$\frac{C_0 - C}{C_0} = B\frac{N_{surf}}{N_{bc}} \quad (2)$$

### 3.6. Band positions

$E_g$ of E80W20 was 0.08 eV smaller than that of E33W67. Semiconductors with similar $E_g$ may not have similar band positions. Based on BEs of XPS Ti 2p, measured band gaps, and some values from literature [24–27], band positions of pure anatase $TiO_2$, S-TO photocatalysts E33W67 and E80W20 were calculated (Fig. 9a–c). For anatase, the difference in ΔE between Ti core line 2p electron binding energy $E_{2p}^{Ti}$ and oxygen valence band maximum $E_{VBM}^{O}$ is 456.19 eV (Eq. (3)), which is also very close to 456.14 eV of

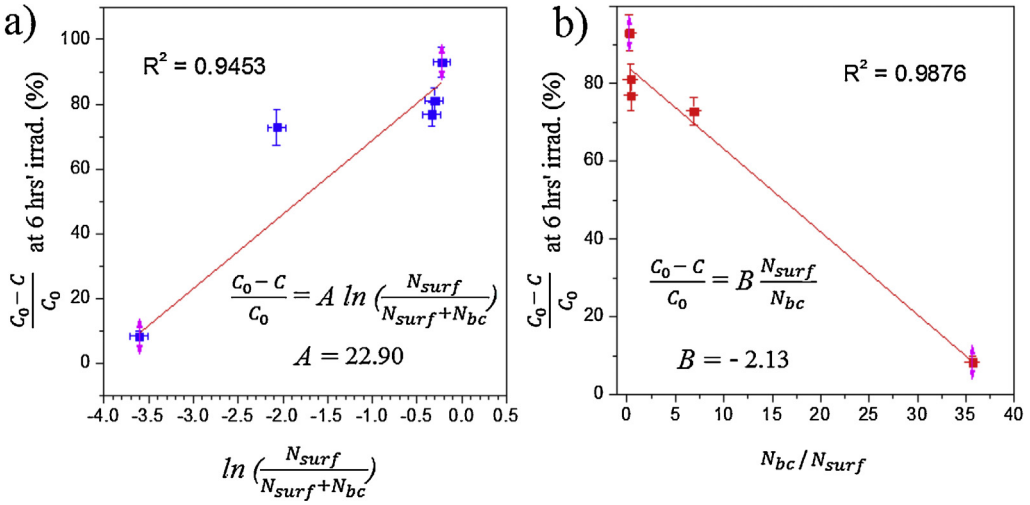


**Fig. 8.** (a) Correlation of surface sulfate species percentage with the DOC degradation efficiency by S-TO catalysts @ 6 h UV irradiation. (b) Correlation of bulk core/surface sulfate species population ratio with the DOC degradation efficiency by S-TO catalysts @ 6 h UV irradiation.

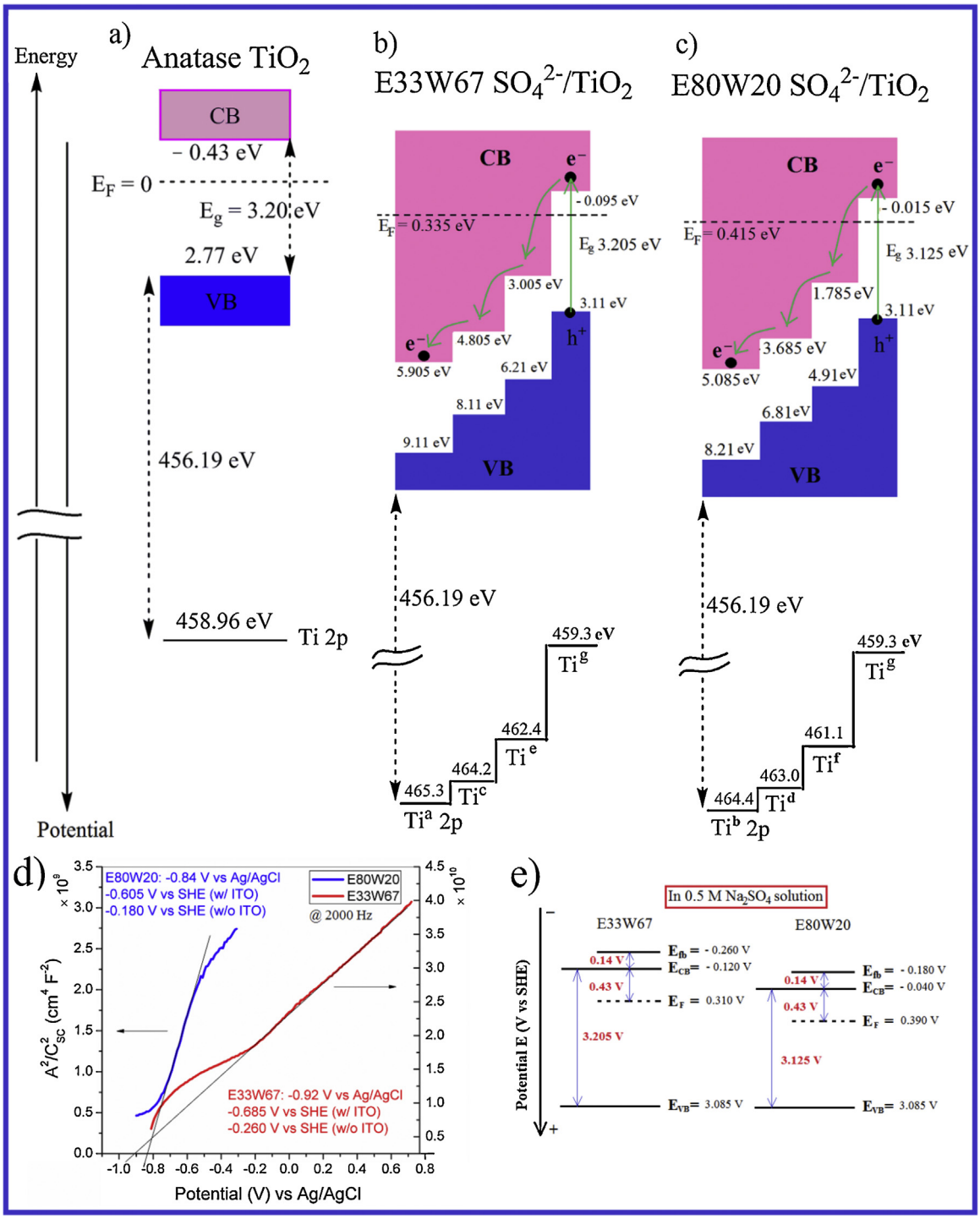


**Fig. 9.** Calculated band positions of (a) pure anatase $TiO_2$, (b) E33W67 S-TO catalyst, and (c) E80W20 S-TO catalyst based on XPS data; (d) Mott-Schottky plots @ 2000 Hz, $E_{fb}$ were derived; Redox potential of Ag/AgCl/1.0 M KCl is + 0.235 eV at 25 °C while that of standard hydrogen electron (SHE) is 0 V at 25 °C; (e) Calculated band positions based on $E_{fb}$. The band positions derived from XPS and $E_{fb}$ agreed each other, confirming the band positions. The band positions illustrated the electron trapping and transferring among the spatial sulfate species.

rutile. According to Scanlon et al. [27], these values still apply even though anatase and rutile form heterojunction. $E_{2p}^{Ti}$ values could be obtained from XPS. However, they needed to be standardized (charge corrected) to C 1 s BE of 285.0 eV as where the ΔE of 456.19 eV was measured (Eq. (4)). In our case, $E_{1s}^{C}$ was 285.5 eV and 285.7 eV for E33W67 and E80W20, respectively. Band gap ($E_g$) was the difference between VB maximum $E_{VBM}^{O}$ (O 2p) and CB lowest edge $E_{3d}^{Ti}$ (Ti 3 d) (Eq. (5)). $E_g$ of 3.20 eV for anatase was taken from literature [27]. Kawakita et al. reported almost constant difference of 0.57 V between $E_{fb}$ and Fermi level ($E_F$) for anatase with random orientation [28]. Scanlon et al. reported the $E_{VBM}$ to be 2.77 eV for anatase with an $E_g$ of 3.20 eV, from where the distance between $E_F$ and $E_{CB}$ could be estimated to be 0.43 V vs standard hydrogen electrode (SHE) (0.43 eV) [27]. In the below equations, ΔE is the

difference between Ti core line 2p electron binding energy $E_{2p}^{Ti}$ and oxygen valence band maximum $E_{VBM}^{O}$, $E_{2p}^{Ti}(std)$ is the Ti 2p BE after standardized, $E_{1s}^{C}$ is the measured C1s BE, and $E_g$ is the band gap.

$$E = E_{2p}^{Ti} - E_{VBM}^{O} = 456.19eV(anatase) \quad (3)$$

$$E_{2p}^{Ti}(std) = E_{2p}^{Ti} - (E_{1s}^{C} - 285.0) \quad (4)$$

$$E_g = E_{VBM}^{O} - E_{3d}^{Ti} \quad (5)$$

Flatband potentials $E_{fb}$ of E33W67 and E80W20 were measured in 0.5 M $Na_2SO_4$ deriving from Mott–Schottky plots (Fig. 9d; SI Fig. S11). Band positions were also calculated from their $E_{fb}$ (Fig. 9e). The calculated band positions from XPS and electrochemical data matched each other, for instance 3.10 eV VBM from XPS data and 3.085 eV VBM from electrochemical data, confirming the corrective of the calculated band positions.

## 4. Discussion

Both E33W67 and E80W20 had four $E_{2p}^{Ti}$ due to four Ti species and therefore four $E_{VBM}^{O}$ and four CB levels were calculated. Electrons at the highest VB (O 2p orbitals in $O^k$ species for E33W67 and $O^j$ species for E80W20) had the highest energies and therefore were most easily excited by photons to the relevant CB (Ti 3d orbitals in $Ti^g$ species for both E33W67 and E80W20) (Fig. 9). Once the electrons were excited to $Ti^g$ species, they were quickly transferred to the lower energy Ti 3 d orbitals nearby, such as from $Ti^g$ to $Ti^a$ via $Ti^e$ and $Ti^c$ in E33W67, and from $Ti^g$ to $Ti^b$ via $Ti^f$ and $Ti^d$ in E80W20. At the lowest Ti 3 d orbitals in $Ti^a$ or $Ti^b$ species, electrons were trapped. Both S-TO photocatalysts E33W67 and E80W20 had the same VB potential of 3.11 V vs SHE. Surface sulfate ions lowered the potential positions of both the CB and VB of S-TO photocatalysts E33W67 and E80W20 compared with those of the pure anatase $TiO_2$. Fig. 9 shows the detailed band positions of pure anatase $TiO_2$, and S-TO catalysts (E33W67 and E80W20). The band positions illustrated the electron trapping and transferring among the spatial sulfate species. When electron was excited by photon from VB to CB, they could be trapped by both surface and bulk core sulfate species, which would compete for the trapping of electrons. Surface sulfate species could trap electrons and easily transfer them to $O_2$ or other oxidants, keeping the catalyst particles electrically neutral. While bulk core sulfate species were not located at the surface and had difficulty to transfer electrons to $O_2$ or other oxidants. Therefore the trapped and accumulated negative electrons in the bulk core lower the electrical potential values of the catalyst particles, making their VB potential values lower and hamper their oxidizing ability to generate •OH radicals. Electron trapping and competition among the spatial sulfate species could rationalize why E33W67 had better and E80W20 had worse photocatalytic activity for organic pollutant degradation than Degussa P25 $TiO_2$.

## 5. Conclusions

We ruled out many possible reasons for the activity difference of E33W67 and E80W20, including crystal phase, size, morphology, SA, pores, $E_g$ and Brönted acid sites. Sulfate species on $TiO_2$ functioned as electron traps and lowered the energies of both the CB and VB of S-TO catalysts (E33W67 and E80W20). Surface sulfate species enhanced activity and bulk core sulfate species hindered it. The electron trapping competition among the spatial sulfate species on S-TO catalysts resulted in a significant impact on their efficiency in photo-degradation of organic pollutants. E33W67 had 12.7% population of surface sulfate species and 87.3% of bulk core sulfate species; While E80W20 had as low as 2.72% population of surface sulfate species and as many as 97.28% of bulk core sulfate species. Due to the fast transit velocity ~1 nm/ps of free photo-excited electrons and much longer trapping time ~500 ps per trap [29], the distribution of these electrons was regulated by the spatial distribution of sulfate species. Bulk core sulfate species trapped electrons but had difficulties to transfer them to the surface for subsequent redox reactions, and therefore negative charge accumulated in the catalyst particles and lowered the potential values of the VB potential obstructing their oxidizing ability to generate •OH radicals. The band positions illustrated electron trapping and transferring among the spatial sulfate species. Correlation of photocatalytic activity and the spatial distribution of sulfate species was established as $(C_0 - C)/C_0 = B \times N_{surf}/N_{bc}$.

## Acknowledgements

This work is supported by the Singapore National Research Foundation under its Environment and Water Technologies Strategic Research Program and administered by the Environment and Water Industry Program Office (EWI) of the PUB on project 1301-IRIS-21 and 1301-IRIS-026. We acknowledge support from the National University of Singapore, National Research Foundation and Economic Development Board (SPORE, COY-15-EWI-RCFSA/N197-1), and Ministry of Education (R-143-000-582-112, and R-and R-143-000-519-112). We thank the Shenzhen Development and Reform Commission (SZ DRC) for supporting our collaborative project with Peking University Shenzhen Graduate School.

## Appendix A. Supplementary data

Supplementary data associated with this article can be found, in the online version, at http://dx.doi.org/10.1016/j.apcatb.2015.02.001.

## References

[1] K. Liu, F.A. Roddick, L.H. Fan, Water Res. 46 (2012) 3229–3239.
[2] A. Perez-Gonzalez, A.M. Urtiaga, R. Ibanez, I. Ortiz, Water Res. 46 (2012) 267–283.
[3] T. Zhou, T.T. Lim, S.S. Chin, A.G. Fane, Chem. Eng. J. 166 (2011) 932–939.
[4] A.Y. Bagastyo, J. Keller, Y. Poussade, D.J. Batstone, Water Res. 45 (2011) 2415–2427.
[5] E. Dialynas, D. Mantzavinos, E. Diamadopoulos, Water Res. 42 (2008) 4603–4608.
[6] M. Lu, S. Kharkwal, H.Y. Ng, S.F.Y. Li, Biosens. Bioelectron. 26 (2011) 4728–4732.
[7] K. Liu, F.A. Roddick, L. Fan, Water Sci. Technol. 63 (2011) 2605–2611.
[8] P. Westerhoff, H. Moon, D. Minakata, J. Crittenden, Water Res. 43 (2009) 3992–3998.
[9] H.L. Yin, Z.Y. Tan, Y.T. Liao, Y.J. Feng, J. Environ. Radioact. 87 (2006) 227–235.
[10] W.Y. Su, Y.L. Chen, X.Z. Fu, K.M. Wei, Chem. J. Chin. Univ. -Chin 23 (2002) 1398–1400.
[11] Y.R. Ma, T.S. Jin, Z.H. Wang, T.S. Li, Indian J. Chem. Sect B-Org. Chem. Incl. Med. Chem. 42 (2003) 1777–1778.
[12] S. Yamazaki, N. Fujinaga, K. Araki, Appl. Catal. A-Gen. 210 (2001) 97–102.
[13] L.K. Noda, R.M. de Almeida, N.S. Goncalves, L.F.D. Probst, O. Sala, Catal. Today 85 (2003) 69–74.
[14] R. Gomez, T. Lopez, E. Ortis-Islas, J. Navarrete, E. Sanchez, F. Tzompanztzi, X. Bokhimi, J. Mol. Catal. A-Chem. 193 (2003) 217–226.
[15] X.Y. Deng, Y.H. Yue, Z. Gao, Appl. Catal. B-Environ. 39 (2002) 135–147.
[16] D.S. Muggli, L.F. Ding, Appl. Catal. B-Environ. 32 (2001) 181–194.
[17] X.H. Lin, S.F.Y. Li, Desalination 344 (2014) 206–211.
[18] X.H. Lin, D. Sriramulu, S. Valiyaveettil, S.F.Y. Li, Water Res. (2014).
[19] P.M. Kumar, S. Badrinarayanan, M. Sastry, Thin Solid Films 358 (2000) 122–130.
[20] O. Carp, C.L. Huisman, A. Reller, Prog. Solid State Chem. 32 (2004) 33–177.
[21] Y. Yamada, H. Yasuda, T. Tayagaki, Y. Kanemitsu, Phys. Rev. Lett. 102 (2009).
[22] H. Yasuda, Y. Yamada, T. Tayagaki, Y. Kanemitsu, Phys. Rev. B 78 (2008).
[23] Y. Tamaki, A. Furube, M. Murai, K. Hara, R. Katoh, M. Tachiya, Phys. Chem. Chem. Phys. 9 (2007) 1453–1460.
[24] R.W. Grant, E.A. Kraut, S.P. Kowalczyk, J.R. Waldrop, J. Vac. Sci. Technol. B 1 (1983) 320–327.

[25] S.P. Kowalczyk, E.A. Kraut, J.R. Waldrop, R.W. Grant, J. Vac. Sci. Technol. 21 (1982) 482–485.
[26] E.A. Kraut, R.W. Grant, J.R. Waldrop, S.P. Kowalczyk, Phys. Rev. B 28 (1983) 1965–1977.
[27] D.O. Scanlon, C.W. Dunnill, J. Buckeridge, S.A. Shevlin, A.J. Logsdail, S.M. Woodley, C.R.A. Catlow, M.J. Powell, R.G. Palgrave, I.P. Parkin, G.W. Watson, T.W. Keal, P. Sherwood, A. Walsh, A.A. Sokol, Nat. Mater. 12 (2013) 798–801.
[28] M. Kawakita, J. Kawakita, Y. Sakka, T. Shinohara, J. Electrochem. Soc. 157 (2010) H65–H68.
[29] Y. Tamaki, A. Furube, M. Murai, K. Hara, R. Katoh, M. Tachiya, J. Am. Chem. Soc. 128 (2006) 416–417.